International Journal of Offshore and Coastal Engineering
Vol. 5 | No. 2 | pp. 50-57 | Nov 2021
e-ISSN: 2580-0914

Submitted: July 08, 2021 | Revised: September 04, 2021 | Accepted: October 13, 2021

Experimental Study and Numerical Analysis of Crane Operability in Floating Crane Catamaran

Rizky Arrico Farhan[a*], Eko Budi Djatmiko[a], Murdjito[a], and Abdul Ghofur[b]

[a)] Department of Ocean Engineering, Sepuluh Nopember Institute of Technology, Surabaya 60111, Indonesia
[b)] BPPT Hydrodynamics Technology Center, Surabaya 60112, Indonesia
[*]Corresponding author: rizkyaaricofarhan@gmail.com

ABSTRACT

Crane vessel is a floating structure equipped with accommodation facilities and one or more cranes to do work in the field. Crane vessel continue to be developed so that they can lift large structures and operate safely in certain environmental conditions. The work that is usually done by crane vessel is to lift heavy or light loads from land to ship, from ship to land, from ship to sea, from sea to ship, and from ship to ship. The process of moving loads carried out by a crane vessel usually called the lifting process. In carrying out its work, a crane vessel is limited by certain criteria for safety reasons. One of them is the criterion that limits the heave motion at the end of the crane boom and roll and pitch motion of the crane vessel. In this final project, an experimental study and numerical analysis of crane operability were carried out on catamaran hulled crane vessel. Experiments were carried out at the Balai Teknologi Hidrodinamika BPPT and numerical analysis using the MOSES software. According to the criteria used, namely Operational Limitations of Offshore Crane Vessels, cranes on floating crane catamaran have the highest operability when the vessel heading is 0^o to the direction of the incoming waves, which is up to H_s 1.45 m.

Keywords: *Crane Vessels, Catamaran, Operability.*

1. INTRODUCTION

The development of oil and gas industry has led to the development of deep-water exploration and exploitation. Besides oil and natural gas, renewable energy such as offshore wind turbine has begun to be realized. The configuration and functionality of the offshore structure are also adjusted with varying environmental conditions. While constructing offshore structure, large cranes is required to move construction elements called modules from the barge or supply vessel onto the platform [1].

A very important subject of offshore crane operations is the impact load which can occur when the load is lifted or unloaded from the transportation barge, due to the difference in vertical velocity of the two floating structures. When the cargo is lifted from the barge, it will make a vertical movement which is determined by the motion characteristics of the vessel crane. On the other hand, the barge also follows wave frequency movements which are generally out of phase with the crane movements on the vessel crane. This can cause damage to the cargo, or the barge, or crane vessel, or even all of those three [1].

In addition to the impact load which is influenced by the response of vertical motion to waves, horizontal movement of vessel cranes is also important in determining an accurate position relative to the platform being built [1].

There are several important aspects that must be reviewed on vessel cranes[1], such as:

- Movement of the crane vertically in waves.
- Horizontal crane positioning accuracy.
- Impact on lifting and lowering loads.
- Deck capacity.
- Transit speed.
- Mooring strength.

Time and cost are closely related to the chosen installation method. To reduce costs and avoid unexpected delays, one of the main challenges is to improve the ability of the floating structures to withstand weather conditions (increase the weather window) [5].

2. LITERATURE REVIEW

Research on various types of offshore crane vessels has been carried out which yield results in the form of operating limitations of several vessel cranes, including crane barges, crane ships, and semisubmersible crane vessels (SSCV) [2]. A crane barge model experiment has been conducted. Experiments were carried out to test the movement of a crane barge when installing modules on FLNG. Tests were

carried out on regular and irregular wave conditions to determine the Response Amplitude Operator (RAO) and the response motion of the two floating structure. Time domain numerical analysis was performed to validate the experimental results [3]. An innovative concept has been developed, namely a catamaran cargo vessel with an on-board crane capable of serving small ports on the coast. This innovation aims to accelerate the movement of containers and general cargo and make marine transportation becoming more competitive [4].

An investigation has been conducted regarding the performance of the operating concept of a wind turbine installation (SPAR floater) using a catamaran hulled vessel. This research focus is to analyze the response of a multibody system (wind turbine - catamaran) under wind and wave loads. Time domain simulations were carried out for the SPAR - catamaran coupling system, SPAR using a passive mooring system, and catamaran using a dynamic positioning system. Under the investigated environmental load, the installation method performed shows an acceptable performance [5].

3. METHODOLOGY

Literature study is carried out, collecting the relevant scientific publications and open literature that can be used as a reference in this research. The collected literature includes previous studies, journals and books that discuss similar problems. Modeling is done using BTH BPPT prototype floating crane catamaran and experimental models using a scale of 1:36. Table 1 shows the main dimensions of the floating crane catamaran.

Table 1. Floating Crane Catamaran Principal Dimension

Principal Dimension			
Parameter	**Full Scale**	**Scale Factor**	**Scale Model**
L_{OA} (m)	111	λ	3.08
L_{WL} (m)	111	λ	3.08
L_{pp} (m)	108	λ	3.00
B (m)	37.8	λ	1.05
H (m)	14.4	λ	0.4
T (m)	4.7	λ	0.13
Displacement (kg)	846400	λ^3	181

The experimental response motion of the floating crane catamaran was carried out in the MOB BTH BPPT laboratory. Table 2 shows the properties of the MOB laboratory.

Table 2. MOB Laboratory Property

Parameter	Value	Unit
Length	45	m
Breadth	30	m
Depth	1.5	m
Maximum Wave Period	0.5 – 3	s
Wave Direction	0 - 90	degree

The main dimensions and hydrostatic properties of the experimental and numerical models will be validated with the prototype, and then the experimental and numerical response spectra will be compared.

The crane operability and response analysis were performed using MOSES software. The results of the analysis of the response to movement and crane operability are compared with the applicable criteria.

4. RESULTS AND DISCUSSION

4.1 Experimental Study

To carry out the experimental studies, the catamaran floating crane must be physically modeled. The scaled model used Froude's law with a scale of 1:36. Model size refers to Table 1. The model used is the BTH BPPT model, as shown in Figure 1. The model is made using balsa wood which is shaped to resemble a scaled lines plan and size. The hull of the model is filled with ballasts in the form of a block-shaped iron plate whose mass is distributed so that the location of the center of gravity (COG) and the radius of gyration of the model match the values that have been scaled. The deck uses plywood and is affixed with passive markers as a reference captured by the motion capture camera.

In the experimental test, the model is attached to a pole that has been arranged in such a way in the test pool. The mooring rope used must be able to withstand the load when the structure is tested so that the structure does not move too far from its original position. The mooring rope selected in the experiment is a steel wire sling with a capacity of 30 lbs.

Figure 1. Experimental model

The mooring system is modeled by assembling several components such as poles, load cells, springs, and steel wire slings. The mooring rope configuration can be seen in Figure 2.

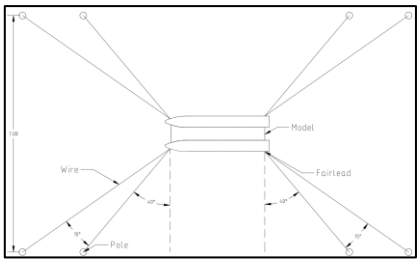

Figure 2. Experimental model mooring system configuration

4.2 Numerical Analysis

Numerical modeling was done using MAXSURF and MOSES software. MAXSURF modeling is done by using the floating crane catamaran lines plan as the background from the MAXSURF perspective, namely the plan, profile, and body plan. The control point on MAXSURF is used as a tools to form a catamaran hull. The model of the floating crane catamaran on MAXSURF can be seen in Figure 3.

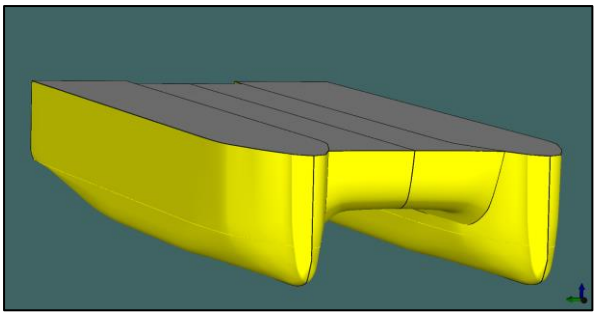

Figure 3. MAXSURF Model

After the model has been created in MAXSURF, the model is imported to the MOSES software for meshing. In this study, the model was meshed with a distance of 1.1 meter because the shape of the catamaran hull is a little more complicated than a typical single hull ship. The meshing results of the model can be seen in Figure 4.

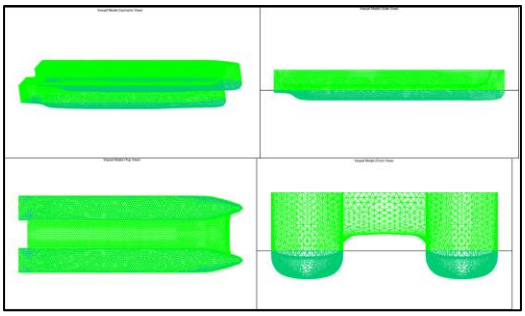

Figure 4. MOSES Meshing

The meshing in MOSES can be used to calculate hydrostatic parameters which will be used as validation between the numerical model and the prototype.

Table 3. Numerical model mooring system configuration

Mooring Configuration						
Properties	Fairlead (m)			Anchor (m)		Angle (°)
	X	Y	Z	X	Y	
ML1	5.64	-15.98	13.15	-200.05	-261.11	-130
ML2	5.64	-15.98	13.15	-256.49	-199.53	-145
ML3	5.64	15.98	13.15	-256.49	199.53	145
ML4	5.64	15.98	13.15	-200.05	261.11	130
ML5	106.50	18.90	13.15	312.19	264.03	50
ML6	106.50	18.90	13.15	368.63	202.45	35
ML7	106.50	-18.90	13.15	368.63	-202.45	-35
ML8	106.50	-18.90	13.15	312.19	-264.03	-50

Table 4. Numerical model mooring properties

Mooring Line Properties		
Description	Value	Unit
Configuration	8 line	
Material	6x19 wire with wire core	
Length	342.87	m
Diameter	5.00	inch
	0.13	m
	127.00	mm
Mass	0.10	ton/m
MBL	16017.41	kN
	1632.76	ton
Pre-tension	198.96	kN
	20.28	ton

The mooring system in numerical modeling is modeled in MOSES. The coordinates of the mooring system configuration can be seen in Table 3. The mooring coordinates refer to the zero point of MOSES which is the bow keel. However, the anchor depth refers to the water surface (80 m). The properties of mooring ropes used in numerical analysis can be seen in Table 4. You can see the visualization of the model moored in Figure 5.

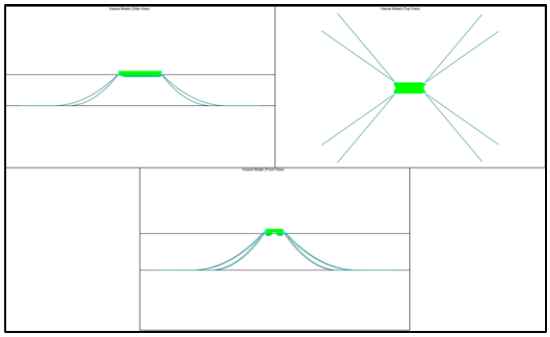

Figure 5. Numerical moored model

4.3 Validation

To obtain results that represent conditions during experimental testing and numerical simulations on MOSES, validation between experimental models, numerical models, and prototypes is necessary. Details about the validated parameters are listed in Tables 5 and 6.

Table 5. Validation between prototypes and experimental models

Prototype – Model Validation, Scale 1:36				
Parameter	Value	Prototype	Model	Error
Disp.	kg	185.31	181.00	2.33%
L_{OA}	m	3.08	3.08	0.00%
L_{WL}	m	3.08	3.08	0.00%
L_{pp}	m	3.00	3.00	0.00%
B	m	1.05	1.05	0.00%
H	m	0.40	0.40	0.00%
T	m	0.13	0.13	0.00%
LCG	m	1.42	1.42	0.00%
VCG	m	0.41	0.41	0.00%
GM	m	1.08	1.08	0.01%
K_{YY}	m	0.77	0.77	0.00%

Table 6. Validation between prototypes and MOSES meshing results

Prototype – MOSES Mesh Validation				
Parameter	**Unit**	**Prototype**	**MOSES**	**Error**
Disp.	**ton**	**8646.00**	**8567.00**	**0.91%**
LOA	**m**	**111.00**	**111.00**	**0.00%**
LWL	**m**	**111.00**	**111.00**	**0.00%**
LPP	**m**	**108.00**	**108.00**	**0.00%**
B	**m**	**37.80**	**37.79**	**0.02%**
H	**m**	**14.40**	**14.40**	**0.00%**
T	**m**	**4.70**	**4.70**	**0.00%**
VCG	**m**	**14.90**	**14.90**	**0.00%**
GM	**m**	**38.95**	**39.69**	**1.91%**

There is an error of 2.33% between the prototype and the experimental model, this is due to the different density of water used where the prototype uses seawater (1.025 tons/m^3) and the experimental model uses fresh water (1.000 tons/m^3). There is an error of 0.91% between the displacement of the MOSES meshing model and the prototype, this is because the meshing quality of MOSES can slightly change the shape of the ship hull.

4.4 Comparison of Response Spectrum from Experimental Study and Numerical Analysis

Numerical analysis of response spectra on a floating crane catamaran was performed using MOSES software. The response spectra of MOSES will be compared with the response spectra of the experiment in one graph. The experimental and numerical response spectra graphs can be seen in Figures 6 to 17.

In the surge motion, there is no significant difference in the response spectra of code 201 considering the increment at the y-axis is too small. In the response spectra of code 202, there is a difference in the location of the peaks of 0.40 rad/s, the peak of the experimental response spectra is at a wave frequency of 0.40 rad/s and the peak of the numerical response spectra is at a wave frequency of 0.80 rad/s.

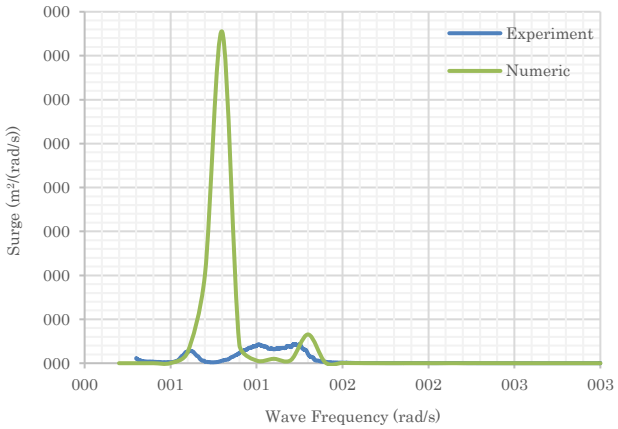

Figure 6. Comparison graph of surge motion response spectra of code 201

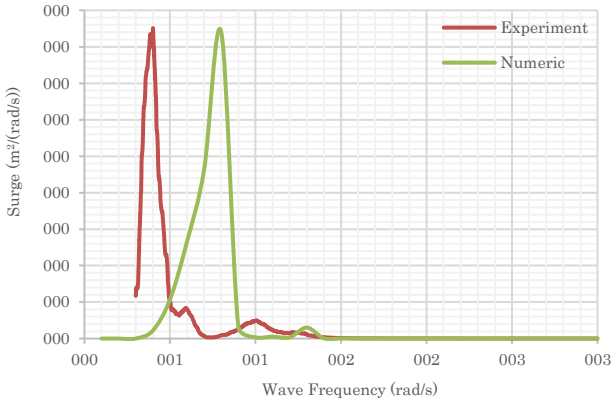

Figure 7. Comparison graph of surge motion response spectra of code 202

In the sway motion, there is a significant difference in peak height in the response spectra of code 201, namely at a wave frequency of 1.00 rad/s. In the response spectra of code 202, there is a significant difference in peak height, namely at the wave frequency of 0.45 rad/s and 1.00 rad/s.

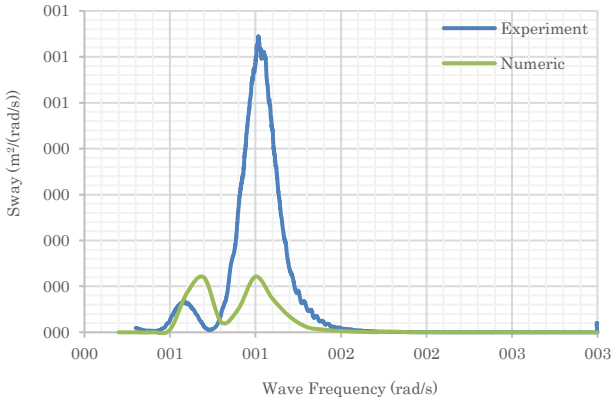

Figure 8. Comparison graph of sway motion response spectra of code 201

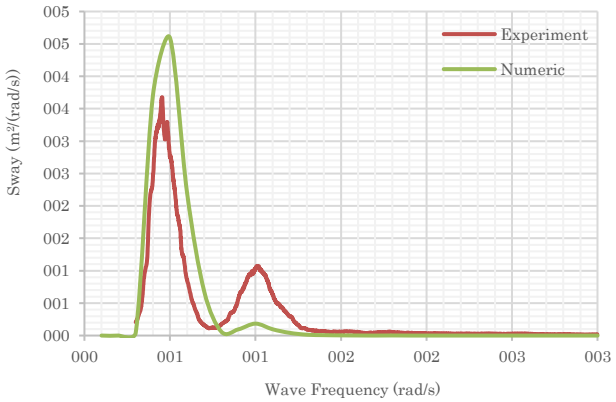

Figure 9. Comparison graph of sway motion response spectra of code 202

In heave motion, there is no significant difference in the two response spectra conditions. In roll motion, there is a significant difference in peak height in the two response spectra conditions.

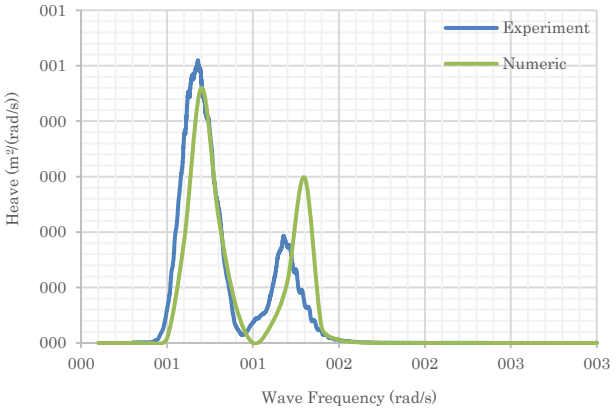

Figure 10. Comparison graph of heave motion response spectra of code 201

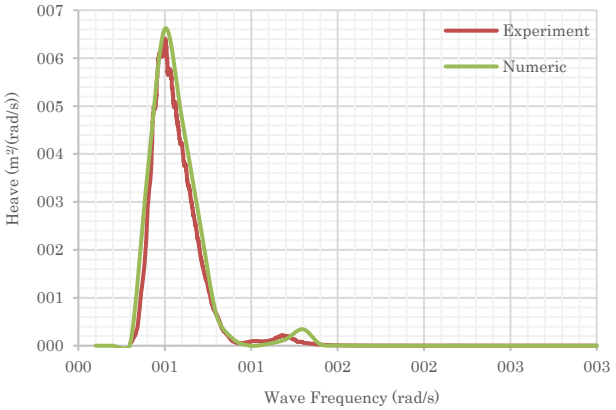

Figure 11. Comparison graph of heave motion response spectra of code 202

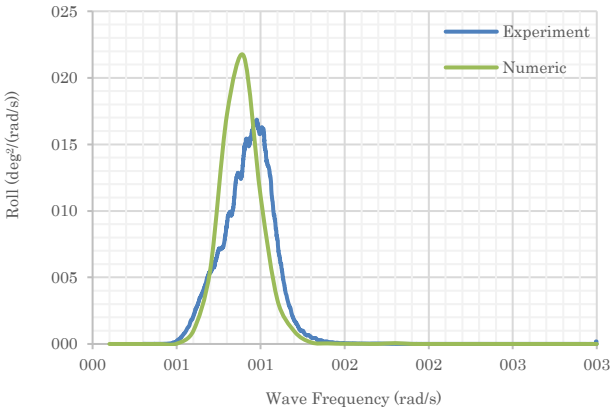

Figure 12. Comparison graph of roll motion response spectra of code 201

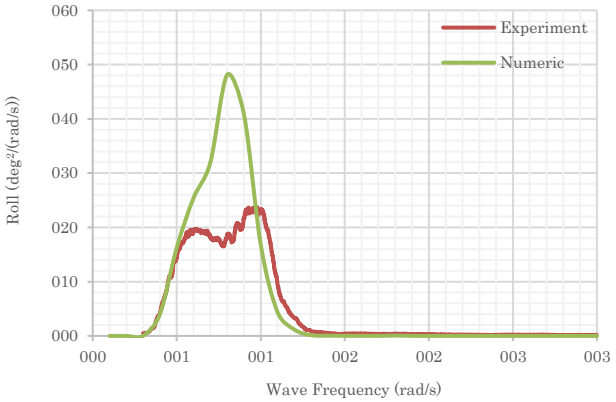

Figure 13. Comparison graph of roll motion response spectra of code 202

In the pitch motion, there is a significant difference in peak height in the response spectra of code 201, especially at the wave frequency of 1.80 rad/s and 1.30 rad/s. In the response spectra of code 202, there is a very significant difference in peak height at a wave frequency of 0.80 rad/s.

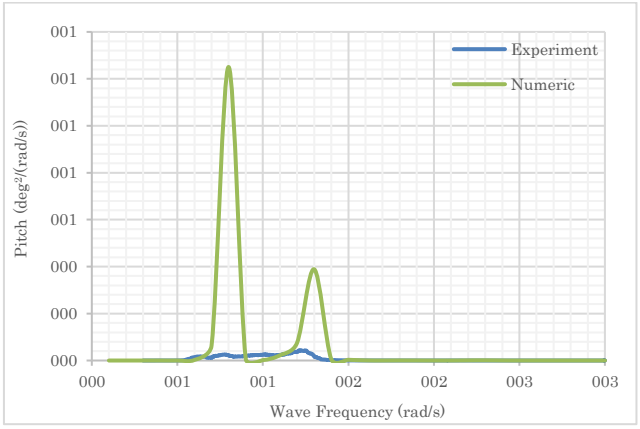

Figure 14. Comparison graph of pitch motion response spectra of code 201

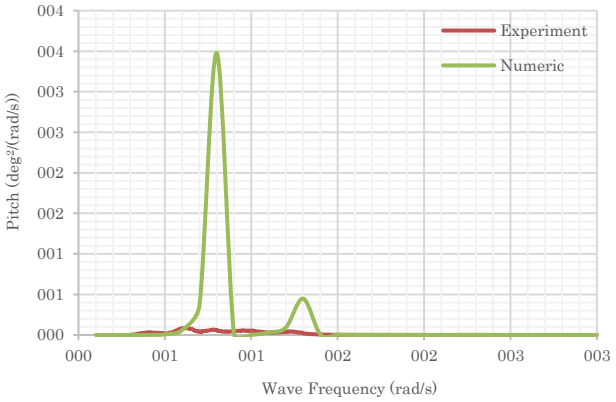

Figure 15. Comparison graph of pitch motion response spectra of code 202

In the yaw motion, there is no significant difference in the two conditions considering the increment on the y-axis is too small. However, the two conditions have different response spectra patterns.

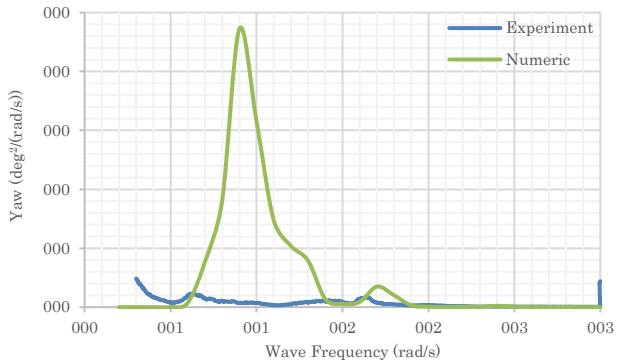

Figure 16. Comparison graph of yaw motion response spectra of code 201

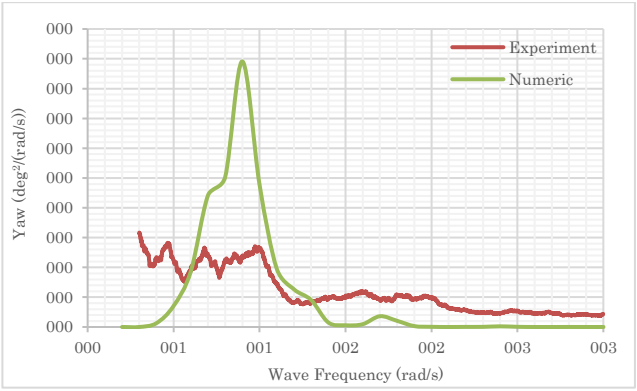

Figure 17. Comparison graph of yaw motion response spectra of code 202

4.5 Crane Operability

The criteria used in determining crane operability use a significant height value or double amplitude as the limit. Double amplitude is obtained from the response spectra. MOSES can produce response spectra statistical results that are currently under review, but it should be noted that MOSES always displays statistical data in the form of single amplitude. Single amplitude needs to be multiplied by 2 first to get double amplitude data.

Significant wave height limits for crane operation for each heading are listed below, however the graphs shown are those which show the operating limitations. The relationship between the significant double amplitude and the crane operating limit can be seen in Figures 18 to 22 and an explanation of the graphs can be seen in Tables 7 to 11.

At heading 0º, the maximum allowable limit for the crane to operate is at H_s 1.45 m. Crane operation is limited by the port side crane aiming 180º at maximum reach radius.

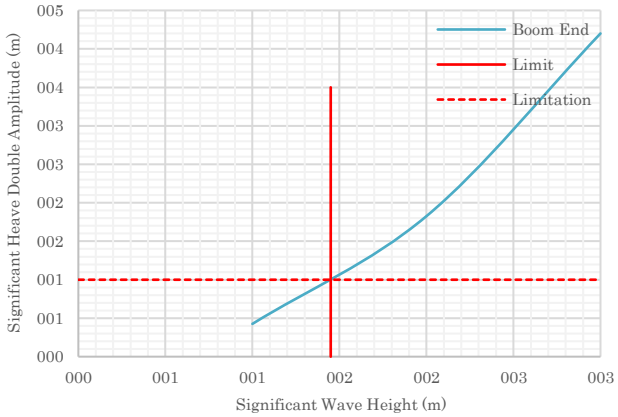

Figure 18. Graph of the relationship between the significant heave double amplitude and the crane operating limit at heading 0º for the PSC4MA code

Table 7. Explanation of the PSC4MA code graph at heading 0º

Operability	
H_s (m)	1.45
PSC4MA	Port Side Crane 180º Maximum Arm

At heading 45º, the maximum allowable limit for the crane to operate is at H_s 1.12 m. Crane operation is limited by the starboard crane aiming 270º at maximum reach radius.

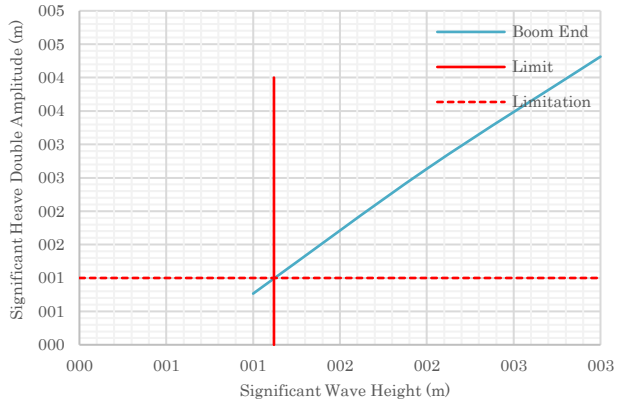

Figure 19. Graph of the relationship between the significant heave double amplitude and the crane operating limit at heading 45º for the SBC2MA code

Table 8. Explanation of the SBC2MA code graph at heading 45º

Operability	
H_s (m)	1.12
SBC2MA	Starboard Crane 270º Maximum Arm

At heading 90º, the maximum allowable limit for the crane to operate is at H_s 0.60 m. Crane operation is limited by the port side crane aiming 90º at maximum reach radius.

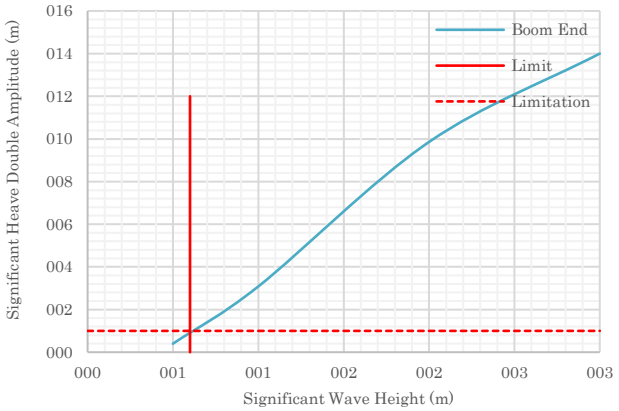

Figure 20. Graph of the relationship between the significant heave double amplitude and the crane operating limit at heading 90º for the PSC2MA code

Table 9. Explanation of the PSC2MA code graph at heading 90º

Operability	
H_s (m)	0.60
PSC2MA	Port Side Crane 90º Maximum Arm

At heading 135º, the maximum allowable limit for the crane to operate is at H_s 1.07 m. Crane operation is limited by the port side crane aiming 90º at maximum reach radius.

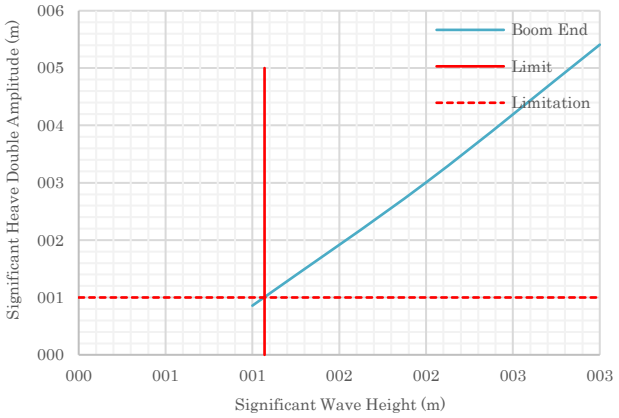

Figure 21 Graph of the relationship between the significant heave double amplitude and the crane operating limit at heading 135º for the PSC2MA code

Table 10 Explanation of the PSC2MA code graph at heading 135º

Operability	
H_s (m)	1.07
PSC2MA	Port Side Crane 90º Maximum Arm

At heading 180º, the maximum allowable limit for the crane to operate is at H_s 1.19 m. Crane operation is limited by the port side crane aiming 180º at maximum reach radius.

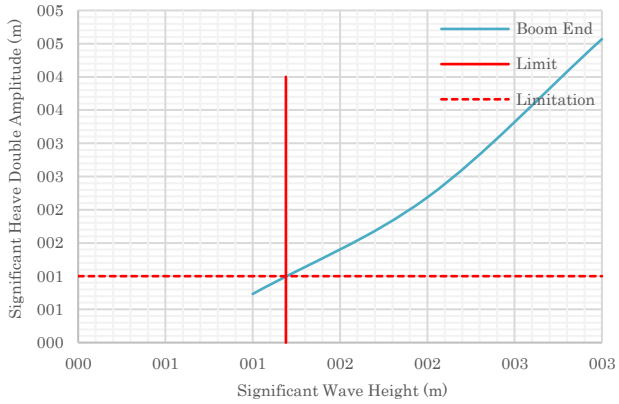

Figure 22. Graph of the relationship between the significant heave double amplitude and the crane operating limit at heading 180º for the PSC4MA code

Table 11. Explanation of the PSC4MA code graph at heading **180º**

Operability	
H_s (m)	1.19
PSC4MA	Port Side Crane 180º Maximum Arm

5. CONCLUSIONS

The conclusions of this study are as follows:

1. The response spectra of the results of numerical analysis and experimentation have different differences depending on the observed mode of motion. In code 201, the pitch motion has the most significant difference compared to the other modes of motion, which is 190.58% error between the significant height of experimental pitch (0.54º) and numerical (1.57º). And in code 202, the pitch motion has the most significant difference compared to the other motion modes, which is 184.33% error between the significant height of the experimental pitch (0.84º) and numerical (2.40º).
2. Several factors that can cause the difference between the response spectra of the results of numerical analysis and experiment are as follows:
   a. Numerical model meshing quality. In this study, MOSES was only able to make meshing of 7800 panels. In certain parts the meshing still looks rough. This can result in differences in the displacement and hull shape between the experimental and numerical scale models. The experimental scale model has a displacement of 8646 tons and the numerical model has a displacement of 8567 tons.
   b. The different hull shape of the numerical model. One of the reasons for the difference in the shape of the hull is that with the same draft (4.7 m) a different displacement is generated

between the experimental scale model and the numerical model. The shape of the hull of the floating building is closely related to the reaction force generated by the floating structures.

c. Differences in the rigidity of the mooring system. In experimental modeling, the stiffness of the mooring system comes from a single spring with constant stiffness, while in the numerical modeling of the mooring system, a catenary is made with a non-constant stiffness.
d. Difference between experimental and numerical wave spectrum.

3. According to the criteria used, which is Operation Limitations of Offshore Crane Vessels - Offshore Technology Conference, crane operability on a floating crane catamaran can be summarized as follows:
    a. The cranes on the floating crane catamaran have the highest operability when the heading vessel is 0^o to the direction of the incoming waves (head seas). The maximum crane can operate up to H_s 1.45 m.
    b. The cranes on the floating crane catamaran have the highest operability when the heading vessel is 90^o to the direction of the incoming waves (beam seas). The maximum crane can operate up to H_s 0.60 m.
    c. From each heading vessel to the direction of the waves, port side cranes and starboard cranes have different operability. This is due to the different location of the crane pedestal from the two cranes. In this research, the location is not symmetrical.

ACKNOWLEDGEMENTS

The author would like to thank the Balai Teknologi Hidrodinamika BPPT for giving the author the opportunity to participate in research on floating crane catamaran.

REFERENCES

[1] Journee, J. M. J. and W. W. Massie. Offshore Hydrodynamic. Delft: Delft University of Technology, 2001.
[2] Clauss, G. F. and T. Riekert. Operational Limitations on Offshore Crane Vessles. Offshore Technology Conference 6217 (1990): 161-170.
[3] Ha, Y. J. et al. Experimental and Numerical Study on Mating Operation of a Topside Module by a Floating Crane Vessel in Waves. Ocean Engineering 154 (2018): 375-388.
[4] Rosenkranz, Volker H. and Carlos Alvarez-Cascos G. Maurino. On-Board STS-Crane on a Catamaran Container Vessel as Combination of Jib- and Gantry-Crane Serving Small Ports, Improving Logistic Efficiency. Procedia – Social and Behavioral Sciences 48 (2012): 3471-3481.
[5] Jiang, Zhiyu et al. Dynamic Response Analysis of a Catamaran Installation Vessel during the Positioning of a Wind Turbine Assembly to a SPAR Foundation. Marine Structure 61 (2018): 1-24.